Control Strategies for Multifunctional Active Front-End Converter in Oil and Gas Platforms

Lorrana F. da Rocha
Graduate Program in Electrical Engineering
Federal University of Minas Gerais (UFMG)
Belo Horizonte, Brazil
Email: lorranafaria@ufmg.br

Lais A. Vitoi
Graduate Program in Electrical Engineering
Federal University of Minas Gerais (UFMG)
Belo Horizonte, Brazil
Email: laisvitoi@gmail

Elisabetta Tedeschi
Department of Electric Power Engineering
Norwegian University of Science and Technology (NTNU)
Trondheim, Norway and
Department of Industrial Engineering
University of Trento
Trento, Italy
Email: elisabetta.tedeschi@ntnu.no

Danilo I. Brandao
Graduate Program in Electrical Engineering
Federal University of Minas Gerais (UFMG)
Belo Horizonte, Brazil
Email: dibrandao@ufmg.br

***Abstract*—This paper compares control strategies for active power exchange and electrical disturbance compensation for multifunction active front-end converters applied to offshore oil and gas platforms. Such scenarios are characterized as weak grids due to their isolated nature and the presence of heavy motor loads. Thereby, harmonic compensation may play an important role in increasing power quality indexes. Thus, different strategies (i.e., sinusoidal current and resistive load synthesis) are compared, varying between injection, absorption and compensation targets. Such functionalities are fully performed by active front-end converters embedded in energy storage system since the bidirectional power exchange is possible; or partially performed by wind-based system, variable frequency drive and active power filter. The strategies are analyzed in terms of damping capacity through the frequency response, voltage distortion caused at the point of the converter connection, total demand distortion for the source current, and power factor at the terminals of the generators.**

***Index Terms*—Multifunctional Converter, O&G Platform, Power Quality, Control Strategies.**

I. Introduction

DESPITE the modification in the world energy matrix over the past few years due to the insertion of renewable sources, the oil and gas (O&G) sector is still among the main sources of energy [1]. Provision and increase of production are guaranteed in the short- and medium-term because of the discovery of new offshore fields located in deep water [2]. The electrical system of an offshore platform is characterized as an isolated grid that has its own generation system, through gas turbines and/or diesel generators, without connection to the onshore power grid.

Fig. 1 illustrates the typical electric grid in an O&G platform. The main components are synchronous generators coupled to the gas turbines, power transformers, short cables, power converters, and loads. This power system is seen as a weak grid, as it has a limited capacity to support deviations in voltage and frequency during the operation. Due to the type of equipment existing in these systems, such as pumps, compressors, and drilling rings, there is a high use of loads with low power quality (PQ) indices with a high level of total harmonic distortion (THD) and a low power factor (PF). In such scenarios, PF can reach minimum values of 0.36, just as THD_v and THD_i can reach values of up to 12% and 27%, respectively [3].

The O&G sector still has a large predominance among the primary energy sources. The integration of renewable sources at the platforms has been proposed as a solution for improving efficiency and reliability of such power system [4]. Connecting renewables into O&G platforms requires the integration of energy storage systems (ESS) due to the fluctuations of power generation [5], [6]. By doing so, it would be possible to insert a multifunction system, capable of operating both for injection and absorption of energy. In addition to providing compensation for reactive and non-linear loads, thus enhancing the PQ of the grid [7]. Such multifunctionalities can be fully performed by active front-end (AFE) converters embedded in ESSs [8]; and partially performed by wind-based systems [9], [10], and variable frequency drives [11], [12].

Harmonic and reactive compensation has been studied in the literature for industrial applications [13], [14] and marine loads [15], [16], and there are even specific applications for the O&G platform, although these are less investigated [17], [18]. In [17], a performance comparison between some harmonics mitigation solutions is presented to determine the optimal mitigation method. In addition, an economical solution is proposed to alleviate the failure mechanisms in adjustable speed drivers in O&G industry without the insertion of expensive harmonic filters. The authors of [18] present the design of a tuned passive filter using genetic algorithm and applied to offshore petrochemical industries. The optimization method is based

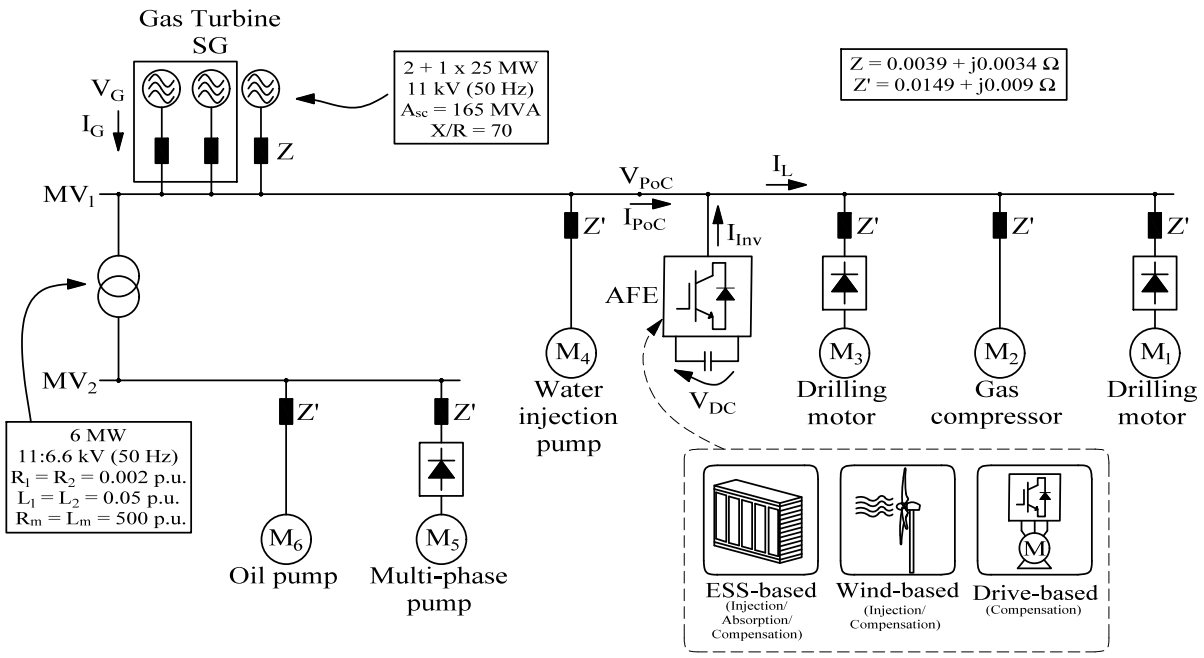

Fig. 1: Schematic diagram of the isolated electric grid of an offshore oil and gas platform.

on minimization of rms source current, harmonic components and reactive power requirement.

Thus, passive filters are a solution for improving PQ on the platform, but they are very bulky elements. On the other hand, active power filters (APFs) have better results in addition to being smaller and lighter. However, they are expensive elements and are not commercially available for medium voltages (11-13.8 kV). A more suitable solution is to use the converters already present on the platform, such as variable frequency drives or battery-storage systems, applied as multifunction AFE converters.

Furthermore, different control strategies have been investigated in literature for the integration of multifunctional converters in the utility grid [19]–[21]. In [19], the use of the instantaneous symmetric component theory is proposed to calculate the reference of current of the multifunctional converter using sinusoidal current synthesis. In addition, a damping filter is integrated with the control algorithm to attenuate fluctuations in the converter currents under operating conditions of variable power. In [20], a control strategy based on direct Lyapunov control theory is used in order to provide a region of adequate stability for the insertion of the distributed generation in the electrical grid. It can reduce stress in the grid by injecting energy distributed during peak demand. In [21], control strategies are presented for a multifunctional inverter using the Conservative Power Theory (CPT), which seeks robustness in terms of system uncertainties and fast dynamic performance on load fluctuations. In this paper, the formulation of the balanced active current term from CPT is used to calculate the references of current for active power injection/absorption and for compensation [22]. This theory makes use of instantaneous measurements of the electrical system, does not require transformation of the frame of reference and is independent of the disturbances of the waveform [23].

Despite the references above, there is a lack of reports for applications in the offshore O&G sector, except for [24] where the control strategies for compensation are investigated. These applications are characterized by high voltage and high rated power converters all operating without connection to the onshore grid. Due to the high harmonic distortion in these scenarios, it is important to know the effect that different control strategies can have at the point of common coupling. Some strategies can provide a greater damping effect for part of the circuit [25], [26]. On the other hand, other strategies for injection/absorption and compensation together can cause greater harmonic distortion and even instability, when compared to the results of the system without the insertion of the converter.

Hence, the contribution of this paper is to analyze the integration of a multifunction converter in an O&G platform, approaching both theoretical investigations, and steady-state and dynamic simulations analysis. In this regard, the paper considers: 1) the frequency response for the analysis of the damping system resonances at a weak grid; and 2) the PQ performance achievable by connecting the multifunction converter for different injection or absorption and compensation targets. For active power injection strategies, sinusoidal current injection and resistive current injection are used, in the same way as for active power absorption. For compensation, two strategies are applied, namely the resistive load synthesis and the sinusoidal current synthesis.

This paper is organized as follows. The main electrical

components and industrial processes that are required in an O&G platform are discussed in Section II. In Section III, the configuration of the multifunctional converter control is described, presenting the equations used to calculate the reference of current for each strategy. Section IV presents the mathematical formulation in the frequency domain for analysis of the damping of resonances in each function of the converter. Section V shows the frequency responses and simulation results. Finally, Section VI concludes the paper.

II. Electrical Model of the O&G Platform

The typical electric circuit of the offshore O&G platform is shown in Fig. 1. The system consists of three gas turbines, one of which is used as a back-up in the event of failure of the two main turbines. The local power generation is responsible for supplying the load demand of the motors from M_1 to M_6 connected on the medium voltage (MV) buses. The turbines are connected in MV_1, 11 kV, along with loads from M_1 to M_4. The loads M_5 and M_6 are connected to the MV_2 bus, with 6.6 kV.

The motors represented in the electrical diagram are typical loads on a platform, responsible for drilling, extracting and injecting fluids into wells. The transformation processes that occur on an O&G platform are described in [24]. These processes require large compressors, pumps and drilling motors with high energy demands, ranging from a few MW to dozens of MW [2], [27]. Some of these motors are connected to electrical converters causing the generation of harmonic components in the circuit. However, these converters make it possible to condition the electric energy and drive with variable speed of some pumps and drilling equipment.

In this regard, passive rectifiers are inserted into the system connected to the motors M_1, M_3, and M_5. In addition, an AFE converter is added to the system for analyzing control strategies for compensation, injection and absorption of energy as detailed in Section III.

III. Control Strategies of the Active Front-End Converter

The AFE converter is controlled for current harmonic mitigation as well as injecting and absorbing active power in an offshore O&G platform. The converter topology is the three-phase two-level voltage source converter and uses passive components, such as a DC-bus capacitor and a LC output filter [28]. The control scheme and the mathematical formulation of the control strategies of the converter are detailed in Subsections III-A and III-B, respectively.

A. Converter control scheme

The converter control diagram contains the outer DC voltage control loop, and a inner current control loop as shown in Fig. 2. C_v and V_{DC}^* represent the controller and the reference for the voltage control, respectively. C_i and i^* represent the controller and the reference for current control in the output filter inductance. The reference generator block calculates the current reference according to the control strategy adopted.

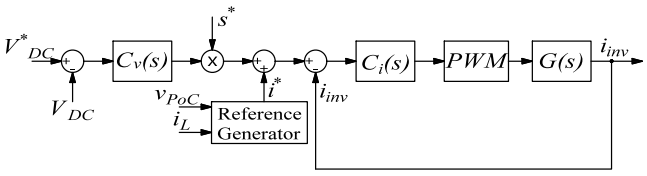

Fig. 2: Block diagram of control scheme applied to multifunction converter.

Moreover, s^* is the synthesis signal that also depends on the control strategy. For strategies with resistive current synthesis, s^* has the same waveform as the voltage at the point of connection (PoC). For strategies with sinusoidal current synthesis, s^* is the fundamental component of V_{PoC} [23].

B. Control strategies for compensation, injection and absorption

Two control strategies can be implemented for both injection and absorption of active power as well as compensation for acting as an shunt APF. Injection strategies are: *i)* sinusoidal current injection (SCI) and *ii)* resistive current injection (RCI). In the absorption of active power the possible strategies are: *i)* sinusoidal current absorption (SCA) and *ii)* resistive current absorption (RCA). The compensation strategies are: *i)* resistive load synthesis (RLS) and *ii)* sinusoidal current synthesis (SCS). The AFE converter is connected to compensate the MV_1 loads M_1, M_2, and M_3 according to analysis of the pre-selection tool shown in [24].

1) Resistive current injection and resistive current absorption strategies: the inverter is capable of operating with multifunctionalities, offering power injection and absorption in addition to support to the grid, which is performed through the compensation of non-linear loads. In the resistive synthesis of the injection and absorption currents, the reference value is generated according to instantaneous voltage values at the point of AFE converter connection. Thus, the reference of current for this strategy is:

$$i_{a,RC}^* = \frac{P^*}{\boldsymbol{V}_{PoC}^2} v_{PoC,m} \tag{1}$$

where $v_{PoC,m}$ is the measured PoC voltage in each phase ($m = a, b, c$), and $\boldsymbol{V}_{PoC}$ is the collective value of the voltage at the PoC, given by $\boldsymbol{V}_{PoC}^2 = V_{PoC,a}^2 + V_{PoC,b}^2 + V_{PoC,c}^2$. P^* is the reference of active power that is injected or absorbed, according to the sign used in the control. The positive sign represents injection and the negative sign represents absorption.

2) Sinusoidal current injection and sinusoidal current absorption strategies: for injection and absorption of sinusoidal active current, it uses an external circuit, such as phase-locked-loop (PLL), to obtain the PoC voltage in the fundamental frequency. The reference of active current (i_a^*) is:

$$i_{a,SC}^* = \frac{P^*}{\boldsymbol{V}_{PoC_1}^2} v_{PoC_1,m} \tag{2}$$

where the subscript $(_1)$ represents the fundamental component of the variables.

3) Resistive load synthesis strategy: results in the resistive behavior of the set of loads (i.e., M_1, M_2, and M_3), so that the current I_{PoC} has the same waveform as the voltage V_{PoC}. The reference of current for RLS compensation is computed as:

$$i^*_{fap,RLS} = i_{L,m} - \frac{P_L}{\boldsymbol{V}^2_{PoC}} v_{PoC,m} \tag{3}$$

where $i_{L,m}$ is the measured load current, and P_L is the active load power.

4) Sinusoidal current synthesis strategy: represents a sinusoidal behavior of the current I_{PoC} according to the fundamental component of V_{PoC}. The reference signal of current for SCS compensation is calculated by:

$$i^*_{fap,SCS} = i_{L,m} - \frac{P_L}{\boldsymbol{V}^2_{PoC_1}} v_{PoC_1,m} \tag{4}$$

5) Total reference signal of current: the current reference of the converter i^*, given by the reference generator block of Fig. 2, is the sum of the compensation current i^*_{fap} and active current i^*_a, then:

$$i^* = i^*_a + i^*_{fap} \tag{5}$$

the current components in each part depend on the strategy used.

IV. Frequency Responses of Converter Functions

This section aims to analyze the frequency response when the AFE converter is controlled for active power injection, active power absorption, and compensation. The simplified model of the circuit is shown in Fig. 3a, where the converter is represented by an ideal current source (I_{INV}). The non-linear loads are simulated by the current sources I_{M1}, I_{M3} and I_{M5}, and the linear loads M_2, M_4 and M_6 are constant impedances. Furthermore, the equivalent single-phase circuit is considered for simplification. The motors M_1, M_2 and M_3 are the loads to be compensated. The impedance Z_C represents the branch of the capacitor at the output terminals of the inverter. The main voltage source V_G is assumed to be ideal, Z_G and $Z^{'}$ represent the line impedances, and Z_T represents the equivalent linkage impedance of the transformer referred to the primary side.

A. Power absorption strategies

Fig. 3b shows the circuit for the power absorption analysis by the AFE converter. The non-linear loads are disturbances in this system and, therefore, are disregarded in this analysis. For SCA strategy, the inverter output current is given by (6) and RCA strategy by (7). Thus, it is established for SCA that the inverter current waveform has only the fundamental component, as considered for the V_G voltage. In the RCA strategy, the current waveform tracks the same shape of the voltage at the PoC.

$$I_{INV} = k\ V_G \tag{6}$$

$$I_{INV} = k_1\ V_{PoC} \tag{7}$$

Note that as the voltage values of the connection point (V_{PoC}) and the source (V_G) are different, due to the line impedance, it is then necessary to use conductances k and k_1 with slight different values.

From these variables (k and k_1) it is possible to obtain the transfer functions (8) and (14) for the RCA and SCA strategies, respectively. The transfer functions indicate the disturbance that the inverter current causes in the PoC voltage V_{PoC} for both strategies of absorption.

$$\frac{V_{PoC-RCA}(s)}{I_{INV-RCA}(s)} = \frac{1}{k_1} \tag{8}$$

Another analysis that can be performed is related to the equivalent impedance seen by the grid indicated in (15) and (16) for SCA and RCA, respectively.

B. Power injection strategies

In the power injection, the equivalent sources of the non-linear loads are also disregarded in the analysis. In addition, the grid is silenced, as shown in the simplified circuit of Fig. 3c, to obtain the gain of V_{PoC} in relation to I_{PoC} due to the influence of the inverter only (i.e., superposition property). The impedance seen by the point of inverter connection is:

$$\frac{V_{PoC-inj}(s)}{I_{PoC-inj}(s)} = Z_G // Z_{M4} // Z_{M6} \tag{9}$$

C. Power compensation strategies

Fig. 3d shows the simplified model for compensation strategies analysis, where the current source I_{M5} represents the non-linear load and Z_{comp} represents the behavior of the AFE converter and the compensated loads (M_1, M_2, and M_3).

For the RLS strategy, the impedance Z_{comp} is computed by:

$$Z_{comp-RLS}(h) = \frac{V_{PoC}(h)}{I_{PoC}(h)} = \frac{1}{k_2} \qquad \forall h, \tag{10}$$

representing a constant behavior for all harmonic components within the converter bandwidth, where h is the harmonic order.

In the SCS strategy, this ratio between voltage and current at the PoC is only valid for the fundamental component due to the sinusoidal behavior of the current. For the other harmonic orders, Z_{comp} is equal to open circuit impedance, such that:

$$Z_{comp-SCS}(h) = \frac{V_{PoC}(h)}{I_{PoC}(h)} = \begin{cases} \frac{1}{k_2}, & \text{for } h = 1 \\ \infty, & \text{for } h \neq 1 \end{cases} \tag{11}$$

The transfer functions of the ratio between V_{PoC} and I_{M5} for SCS and RLS are given by (12) and (13), respectively.

$$\frac{V_{PoC-h_{SCS}}(s)}{I_{M5-h_{SCS}}(s)} = Z_G // Z_{M4} // Z_{M6} // Z_C \tag{12}$$

$$\frac{V_{PoC-h_{RLS}}(s)}{I_{M5-h_{RLS}}(s)} = Z_G // Z_{M4} // Z_{M6} // Z_C // (1/k_2) \tag{13}$$

$$\frac{V_{PoC-SCA}(s)}{I_{INV-SCA}(s)} = \frac{[kZ_G+1][Z_{M6}Z_{M4}Z_CZ_{M2}]}{k[Z_{M6}Z_{M4}Z_CZ_{M2}+Z_GZ_{M4}Z_CZ_{M2}+Z_GZ_{M6}Z_CZ_{M2}+Z_GZ_{M6}Z_{M4}Z_{M2}+Z_GZ_{M6}Z_{M4}Z_C]} \quad (14)$$

$$\frac{V_{G-SCA}(s)}{I_{G-SCA}(s)} = \frac{Z_{M6}Z_{M4}Z_CZ_{M2} + Z_GZ_{M4}Z_CZ_{M2} + Z_GZ_{M6}Z_CZ_{M2} + Z_GZ_{M6}Z_{M4}Z_{M2} + Z_GZ_{M6}Z_{M4}Z_C}{Z_{M4}Z_CZ_{M2} + Z_{M6}Z_CZ_{M2} + Z_{M6}Z_{M4}Z_C + Z_{M6}Z_{M4}Z_{M2} - kZ_{M6}Z_{M4}Z_CZ_{M2}} \quad (15)$$

$$\frac{V_{G-RCA}(s)}{I_{G-RCA}(s)} = Z_G + \left[\frac{Z_{M6}Z_{M4}Z_C(1/k_1)Z_{M2}}{Z_{M4}Z_C(1/k_1)Z_{M2} + Z_{M6}Z_C(1/k_1)Z_{M2} + Z_{M6}Z_{M4}(1/k_1)Z_{M2} + Z_{M6}Z_{M4}Z_CZ_{M2} + Z_{M6}Z_{M4}Z_C(1/k_1)}\right] \quad (16)$$

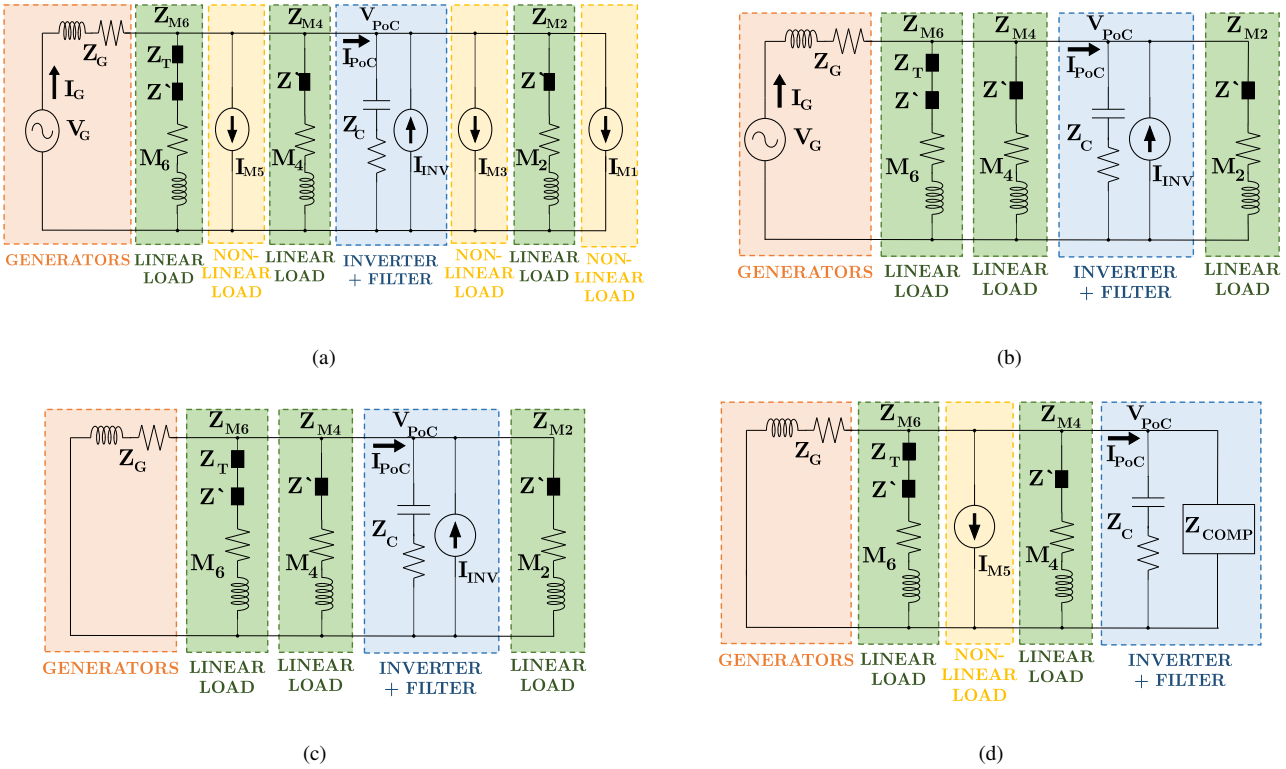

Fig. 3: Equivalent circuit model: (a) Simplified, (b) Absorption, (c) Injection and (d) Compensation.

V. Simulation Results

This section shows the results obtained by means of MATLAB/Simulink program considering the whole power system, as in Fig. 1. These results are presented in two separate analysis: *i)* the system frequency responses compared to the simplified transfer functions obtained in Section IV, and *ii)* the PQ performance indices for the operating modes of the converter considering different strategies (i.e., injection, absorption and compensation). The parameters of Fig. 1 are shown in Table I.

TABLE I: Parameters of the loads of Fig. 1.

Load	Type	Active power	PF	Apparent power	$\sqrt{A^2-P^2}$
M_1	Drilling motor	5 MW	0.95	5.36 MVA	1.93 MVA
M_2	Gas compressor	4 MW	0.85	4.71 MVA	2.48 MVA
M_3	Drilling motor	5 MW	0.95	5.35 MVA	1.90 MVA
M_4	Water injection pump	4 MW	0.8	5.00 MVA	3.00 MVA
M_5	Multi-phase pump	2 MW	0.95	2.10 MVA	0.64 MVA
M_6	Oil pump	1 MW	0.6	1.67 MVA	1.33 MVA

A. Frequency response results

The theoretical transfer functions obtained in Section IV are plotted and compared with the circuit simulation results. The values used in the impedances are detailed in Table II.

1) Power absorption strategies: the bode diagrams of the functions (8) and (14) are shown in Fig. 4a. These transfer functions indicate voltage response V_{PoC} in relation to the current absorbed by the converter. It can be seen that for the fundamental frequency (50 Hz) the two strategies behave similarly. The frequency response shows that the circuit has greater gains from 1220 Hz for the RCA strategy. However, the SCA strategy has a resonance peak at approximately 850 Hz. This shows that the SCA amplifies the current harmonics around this frequency. For RCA the voltage behavior is constant with respect to the current I_{INV} and is given according to the point $1/k_1$, with the conductance as $k_1 = 0.0468$ S. This value is obtained based on the operating point of the SCA circuit at 50 Hz. The comparison of the results shows that the RCA strategy is more suitable than SCA for the absorption of active power.

The points in Fig. 4a are the results of the simulated

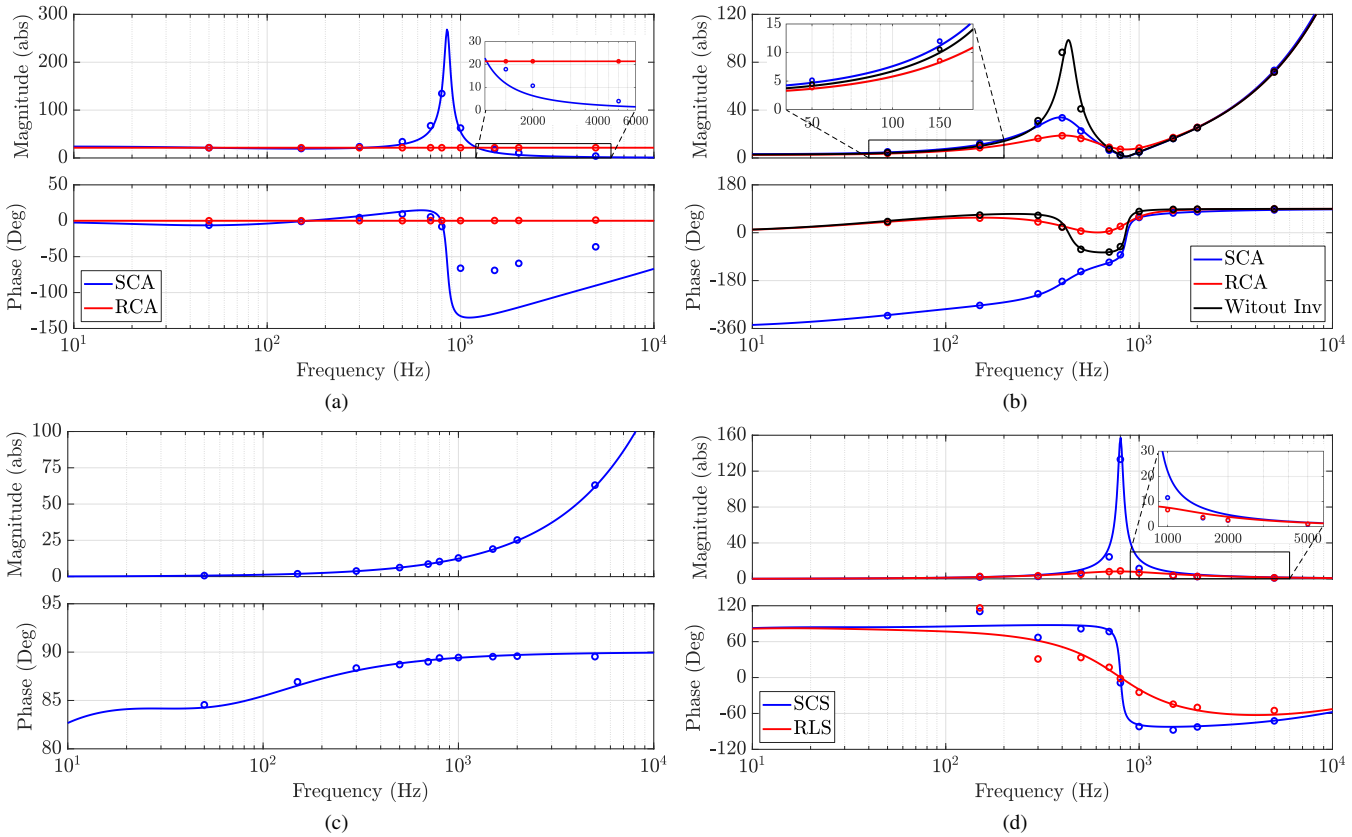

Fig. 4: Bode Diagram: (a) Absorption of $V_{PoC}(s)/I_{INV}(s)$, (b) Absorption of $V_G(s)/I_G(s)$, (c) Injection of $V_{PoC}(s)/I_{PoC}(s)$ and (d) Compensation of $V_{PoC-h}(s)/I_{M5-h}(s)$.

TABLE II: Simulation values to plot the Bode diagram of Fig. 4.

Variable	Value
k	0.0413 S
k_1	0.0468 S
k_2	0.1150 S
$Z_G = Z + Z_{generator}$	14.34 + j734.20 mΩ
$Z_{M2} = Z' + Z_{motor2}$	7.27 + j4.54 Ω
$Z_{M4} = Z' + Z_{motor4}$	6.47 + j4.85 Ω
$Z_{M6} = Z' + Z_T + Z_{motor6}$	14.66 + j21.40 Ω
Z_C	0.5 + j159.15 Ω

complete system. One can see that the simulation points follow the trend represented by the transfer functions of $V_{PoC}(s)/I_{INV}(s)$ for absorption, despite the simplifications considered in the circuit of Fig. 3b. The resonance peak of the SCA strategy is greater in the theoretical plot, since the simulation considers certain components (e.g., series resistance in cables and transformer) in its mathematical modeling, thus providing more damping for the system.

Fig. 4b shows the frequency response of equivalent impedance, (15) and (16), for absorption analysis. The RCA strategy provides more damping to the system than SCA up to 600 Hz. The curve without the inverter shows that the system has a resonance around 430 Hz, which is attenuated by the absorption of power by the inverter. In addition, the phase variation is more pronounced for SCA. Fig. 4b also shows the results of the simulation through the points added in the bode diagram. At these simulation points, the non-linear loads are disregarded, as they affect the current drained from the source but are not included in the transfer function of the model.

2) Power injection strategies: the impedance seen by the PoC, given by (9), is shown in the bode diagram of Fig. 4c. This analysis indicates how the PoC is affected by the current injected by the AFE converter. Signal amplification is observed for frequencies above 100 Hz, which may cause distortions in V_{PoC}. Such slope is also noted by the simulation points obtained. As shown in Fig. 4c, SCI strategy at 50 Hz is more suitable than RCI strategy, which considers in the current waveform the voltage harmonic components in addition to the fundamental one. In this simulation, the current source I_{M_5}, which represents the disturbance (i.e., non-linear load), is neglected as per the theoretical analysis in Subsection IV-B.

3) Power compensation strategies: considering (12) and (13), it is possible to obtain the frequency responses shown in 4d. As can be seen, the RLS strategy provides more damping effect for harmonic currents than SCS at frequencies around 800 Hz. The gains obtained in the harmonics points of the system through the simulation are shown in the Fig. 4d, where it is possible to notice the tendency of the resonance peak for the SCS strategy curve.

B. Power quality performance analysis

The performance analysis of PQ is carried out to compare the response of the system to different injection/absorption and compensation strategies. The PQ indices used are THD for voltage of the PoC, total demand distortion (TDD) for the source current, and PF at the terminals of the generators according to the data shown in Table III. The values show that the PQ indices prior the insertion of the AFE is 10.33% for THD_v, 10.59% for TDD_i, and 0.9087 for PF. With the active filter function, the circuit obtains a better PQ gain for the RLS, which offers greater damping for the system in terms of harmonic current than SCS.

When only the injection is considered in the converter, there is a resonance for the RCI strategy, which makes the system distortion very high and PF low. In this strategy, the reference of the injected current has the same harmonic components as V_{PoC}, accentuating the oscillation of the system at the common coupling point. This characteristic is shown in the frequency response. With SCI, the THD_v is measured and equal to 13.76%, being the best strategy for the injection.

In the active power absorption function, without compensation, the RCA is more suitable, with lower THD_v values than SCA strategy. Thus, the system sees the inverter as another resistive load, proportionally decreasing the distortion in relation to the system without inverter.

The following analysis in Table III shows the same conclusions obtained by the analysis of the transfer functions, where the strategy of RLS, SCI and RCA are better for the comparisons described. The RLS strategy with the RCA obtained the lowest distortion value for the simulated values in the active power absorption and compensation mode. For injection and compensation, the best result was RLS and SCI. These conclusions are also evidenced qualitatively by the waveforms shown in Fig. 5, where less distorted forms are perceived for the best strategies.

TABLE III: Power quality analysis for multifunctional converter control strategies.

Compensation Strategies	Inj./Abs. Strategies	$\text{THD}_{V_{PoC}}$ (%)	TDD_{I_G} (%)	FP
-	-	10.33	10.59	0.9087
SCS	-	7.05	3.14	0.9802
RLS	-	2.22	1.50	0.9832
-	SCI	13.76	12.11	0.8637
-	RCI	High	High	Low
-	SCA	13.54	11.94	0.9413
-	RCA	10.74	11.10	0.9483
SCS	SCI	7.10	3.16	0.9683
	RCI	High	High	Low
RLS	SCI	2.23	1.49	0.9717
	RCI	2.74	1.69	0.9715
SCS	SCA	6.98	3.14	0.9861
	RCA	3.46	1.95	0.9883
RLS	SCA	2.21	1.52	0.9888
	RCA	1.90	1.37	0.9889

VI. Conclusion

This paper investigated different control strategies for multifunctional active front-end converter injecting or absorbing active power and compensating harmonics. The electrical system analyzed was referred to the O&G platform, being characterized as an isolated system, with high energy consumption and low power quality indices.

For compensation strategies, it has been shown that the RLS strategy obtained a THD_v value three times smaller and a TDD_i value half than the SCS strategy, for the case study carried out herein. In the other scenarios, considering absorption or injection concomitantly with compensation, the best power quality indices values were obtained using the RLS strategy. Regarding injection strategies, it was observed that the RCI strategy is not suitable for the O&G power system, as it amplifies the high frequency components. It resulted in very high harmonic content in the two simulated scenarios. For the scenarios considering absorption, the RCA strategy performed better, with 20% lower THD_v value than SCA, which means that absorbing active power following the voltage waveform provides damping like a resistor at the end of a feeder.

Moreover, this paper showed that using the proper strategies for the active front end converter embedded in energy storage system, wind-based system or variable frequency drive can bring appealing results in terms of power quality enhancement. Specially for the electrical systems on O&G platforms, where reactive and harmonic compensation is usually required. Finally, the RLS, SCI and RCA strategies are suggested for O&G applications, because they provide more damping to the system than the others strategies, SCS, RCI and SCA.

Acknowledgment

This research was partly funded under the program PETROMAKS2 of the Research Council of Norway, within the project "Smart Platform" (grant number 308735).

References

[1] World Energy Outlook 2019. International Energy Agency. Accessed December, 2020. [Online]. Available: https://www.iea.org/reports/world-energy-outlook-2019

[2] K. Rajashekara, H. S. Krishnamoorthy, and B. S. Naik, "Electrification of subsea systems: requirements and challenges in power distribution and conversion," *CPSS Transactions on Power Electronics and Applications*, vol. 2, no. 4, pp. 259–266, 2017.

[3] F. D. K. Schipman, "The importance of good power quality," in *ABB Power Qual. Prod*, 2010, pp. 1–20.

[4] R. N. Fard and E. Tedeschi, "Integration of distributed energy resources into offshore and subsea grids," *CPSS Transactions on Power Electronics and Applications*, vol. 3, no. 1, pp. 36–45, 2018.

[5] M. H. Nehrir, C. Wang, K. Strunz, H. Aki, R. Ramakumar, J. Bing, Z. Miao, and Z. Salameh, "A review of hybrid renewable/alternative energy systems for electric power generation: Configurations, control, and applications," *IEEE Transactions on Sustainable Energy*, vol. 2, no. 4, pp. 392–403, 2011.

[6] J. Tan and Y. Zhang, "Coordinated control strategy of a battery energy storage system to support a wind power plant providing multi-timescale frequency ancillary services," *IEEE Transactions on Sustainable Energy*, vol. 8, no. 3, pp. 1140–1153, 2017.

[7] L. B. G. Campanhol, S. A. O. da Silva, A. A. de Oliveira, and V. D. Bacon, "Power flow and stability analyses of a multifunctional distributed generation system integrating a photovoltaic system with unified power quality conditioner," *IEEE Transactions on Power Electronics*, vol. 34, no. 7, pp. 6241–6256, 2019.

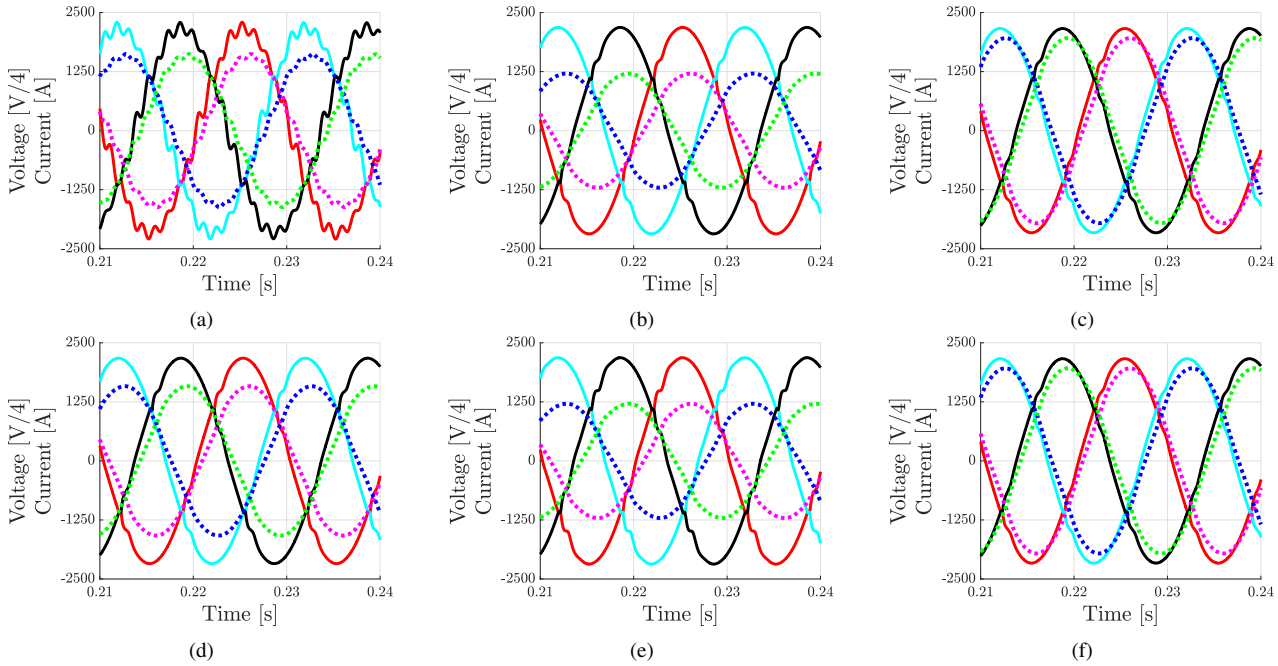

Fig. 5: Analysis of V_{PoC} and I_G waveform: (a) SCS strategy without injection/absorption of active power, (b) RLS strategy and SCI strategy (c) RLS strategy and SCA strategy, (d) RLS strategy without injection/absorption of active power, (e) RLS strategy and RCI strategy and (f) RLS strategy and RCA strategy.

[8] Gamesa Electric. Battery Inverters: Stor 3X series – PCS. Accessed March, 2021. [Online]. Available: https://www.gamesaelectric.com/producto/stor-3x-series-pcs-battery-inverters/

[9] ABB. Medium Voltage Wind Turbine Converter: PCS6000. Accessed March, 2021. [Online]. Available: https://new.abb.com/power-converters-inverters/wind-turbines/utility-scale/pcs6000

[10] Siemens Gamesa. Offshore Wind Turbine: SG 8.0-167 DD. Accessed March, 2021. [Online]. Available: https://www.siemensgamesa.com/en-int/products-and-services/offshore/wind-turbine-sg-8-0-167-dd

[11] GE Power Conversion. Medium Voltage AC Drive: MV7000 Press Pack. Accessed March, 2021. [Online]. Available: https://www.gepowerconversion.com/product-solutions/medium-voltage-drives/mv7000

[12] ABB. Medium Voltage AC Drive: ACS2000. Accessed March, 2021. [Online]. Available: https://new.abb.com/drives/medium-voltage-ac-drives/acs2000

[13] M. Kale and E. Özdemir, "Harmonic and reactive power compensation with shunt active power filter under non-ideal mains voltage," *Electric Power Systems Research*, vol. 74, no. 3, pp. 363–370, 2005.

[14] V. A. Shankar and N. S. Kumar, "Implementation of shunt active filter for harmonic compensation in a 3 phase 3 wire distribution network," *Energy Procedia*, vol. 117, pp. 172–179, 2017.

[15] D. Kumar and F. Zare, "A comprehensive review of maritime microgrids: System architectures, energy efficiency, power quality, and regulations," *IEEE Access*, vol. 7, pp. 67 249–67 277, 2019.

[16] C. Su and C. Hong, "Design of passive harmonic filters to enhance power quality and energy efficiency in ship power systems," in *49th IEEE/IAS Industrial Commercial Power Systems Technical Conference*, 2013, pp. 1–8.

[17] K. Lee, D. Carnovale, D. Young, D. Ouellette, and J. Zhou, "System harmonic interaction between dc and ac adjustable speed drives and cost effective mitigation," *IEEE Transactions on Industry Applications*, vol. 52, no. 5, pp. 3939–3948, 2016.

[18] V. Verma and B. Singh, "Genetic-algorithm-based design of passive filters for offshore applications," *IEEE Transactions on Industry Applications*, vol. 46, no. 4, pp. 1295–1303, 2010.

[19] N. R. Tummuru, M. K. Mishra, and S. Srinivas, "Multifunctional vsc controlled microgrid using instantaneous symmetrical components theory," *IEEE Transactions on Sustainable Energy*, vol. 5, no. 1, pp. 313–322, 2014.

[20] E. Pouresmaeil, M. Mehrasa, and J. P. S. Catalão, "A multifunction control strategy for the stable operation of dg units in smart grids," *IEEE Transactions on Smart Grid*, vol. 6, no. 2, pp. 598–607, 2015.

[21] A. Mortezaei, M. G. Simões, A. S. Bubshait, T. D. C. Busarello, F. P. Marafão, and A. Al-Durra, "Multifunctional control strategy for asymmetrical cascaded h-bridge inverter in microgrid applications," *IEEE Transactions on Industry Applications*, vol. 53, no. 2, pp. 1538–1551, 2017.

[22] P. Tenti, H. K. M. Paredes, and P. Mattavelli, "Conservative power theory, a framework to approach control and accountability issues in smart microgrids," *IEEE Transactions on Power Electronics*, vol. 26, no. 3, pp. 664–673, 2011.

[23] F. P. Marafão, D. I. Brandão, A. Costabeber, and H. K. M. Paredes, "Multi-task control strategy for grid-tied inverters based on conservative power theory," *IET Renewable Power Generation*, vol. 9, no. 2, pp. 154–165, 2015.

[24] L. A. Vitoi, D. Brandao, and E. Tedeschi, "Active power filter preselection tool to enhance the power quality in oil and gas platforms," *Energies*, vol. 14, no. 4, 2021.

[25] T. E. Nunez-Zuniga and J. A. Pomilio, "Shunt active power filter synthesizing resistive loads," *IEEE Transactions on Power Electronics*, vol. 17, no. 2, pp. 273–278, 2002.

[26] M. I. M. Montero, E. R. Cadaval, and F. B. Gonzalez, "Comparison of control strategies for shunt active power filters in three-phase four-wire systems," *IEEE transactions on power electronics*, vol. 22, no. 1, pp. 229–236, 2007.

[27] T. Waterfield and B. Germaine, "The world's injection pumps." *Sulzer Technical Review*, vol. 85, no. 4, pp. 8–11, 2003.

[28] D. Solatialkaran, F. Zare, T. K. Saha, and R. Sharma, "A novel approach in filter design for grid-connected inverters used in renewable energy systems," *IEEE Transactions on Sustainable Energy*, vol. 11, no. 1, pp. 154–164, 2020.